International Journal of Biological Macromolecules 320 (2025) 145668

Contents lists available at ScienceDirect

International Journal of Biological Macromolecules

journal homepage: www.elsevier.com/locate/ijbiomac

Structural and functional insights into Gp21 as a new SF4 helicase of prolate-headed *Lactococcus lactis* phage 94p4

Anna Santo [a], Magdalena Chmielewska-Jeznach [a,b], Kamil Steczkiewicz [a], Tamara Aleksandrzak-Piekarczyk [a], Agnieszka K. Szczepankowska [a,*]

[a] Institute of Biochemistry and Biophysics, Polish Academy of Sciences, Pawińskiego 5a, 02-106 Warsaw, Poland
[b] Medical University of Warsaw, Department of Medical Biology, Litewska 14/16, 00-575 Warsaw, Poland

ARTICLE INFO

Keywords:
SF4 helicase
Replication protein
DNA unwinding
Lytic bacteriophage
Ceduovirus
Prolate-headed
Lactococcus lactis

ABSTRACT

The Gp21 protein is encoded in the early gene region of the lytic, prolate-headed (*Ceduovirus* type) *Lactococcus lactis* bacteriophage 94p4 genome. By *in silico* modelling we found that the protein shares significant structural and motif-specific homology with superfamily 4 (SF4) replicative helicases, such as *Escherichia coli* DnaB, phage T4 Gp41, and phage T7 Gp4. Our study demonstrates that Gp21 possesses robust DNA unwinding activity, efficiently separating strands of DNA heteroduplexes in a 5′ to 3′ direction. Biochemical characterization revealed that Gp21 forms hexamers and requires ATP and Mg^{2+} as cofactors for optimal activity. Site-directed mutagenesis of conserved residues within Gp21 impaired both its unwinding activity and hexamer formation, further supporting its classification as an SF4 helicase. The functional and structural similarity of Gp21 to SF4 replicative DNA helicases strongly suggests its role in DNA replication. This discovery identifies Gp21 as the first functionally confirmed SF4 helicase in *Ceduovirus* phages, offering new insights into the replication of this phage family.

1. Introduction

Ceduoviruses (or c2-type) are prolate-headed lytic phages that infect *Lactococcus lactis* bacteria, making them one of the most dominant phage groups in dairy environments and a significant threat to dairy production [1]. Despite the challenges posed by phage proliferation in dairy plants, there have been relatively few studies on the mechanisms and proteins engaged in *Ceduovirus* propagation. Like other *L. lactis* phages, Ceduoviruses have double-stranded (ds) DNA genomes and a modular genome organization resembling that of dsDNA lambdoid phages [2,3]. These common traits suggest that these two phage groups might share similar replication mechanisms. Dairy-associated *L. lactis* bacteriophages, including Ceduoviruses, exhibit a relatively fast replication rate, which indicates efficient phage multiplication [4,5]. However, the proteins and DNA elements essential for the propagation of *Lactococcus* phages are not fully known. The origin of *Ceduovirus* phage replication (ori) has been identified within a 611-bp noncoding A-T rich region located between the oppositely oriented early and late gene regions [6]. Callanan et al. [7] demonstrated that the replication of a model *L. lactis Ceduovirus* phage c2 initiates at the ori and proceeds *via* the theta mode, with possible later involvement of another undefined ori-independent mechanism. Further studies also revealed that phage c2 replication does not require an initiation protein, such as for phage lambda, or any other phage-encoded proteins, but rather relies on the transcript of the early promoter P_E1, located within the ori region [7,8]. Since then, several studies have examined the ori region of Ceduoviruses, and a DNA single-stranded binding protein with putative accessory role in phage replication was characterized [5,9,10]. However, a detailed understanding of *Ceduovirus* replication initiation and the proteins directly involved in this process remains elusive. Weigel and Seitz [11] analyzed replication modules in phages of gram-positive and gram-negative hosts, categorizing them based on three major gene products: initiator, DNA helicase, and helicase loader. A lack of one or more of these functions can often be compensated by host-encoded proteins.

The initiator protein (*e.g.*, O protein in phage lambda or DnaA in *Escherichia coli*) triggers phage replication by binding and partially melting the A-T rich dsDNA ori region, facilitating replisome formation [12]. The helicase loader (*e.g.*, P protein in phage lambda or DnaC in *E. coli*) assists by loading the DNA helicase onto the DNA [13]. The DNA helicase (*e.g.*, Gp41 in phage T4 or DnaB in *E. coli*) unwinds the dsDNA,

* Corresponding author.
E-mail address: agaszczep@ibb.waw.pl (A.K. Szczepankowska).

https://doi.org/10.1016/j.ijbiomac.2025.145668
Received 20 December 2024; Received in revised form 11 June 2025; Accepted 29 June 2025
Available online 1 July 2025

separating the complementary DNA strands and forming the replication fork [14,15].

Investigation into the replication modules of *Lactococcus* phages, based on P335-type phages, revealed that they possess genes encoding either only the initiator protein or both the initiator protein and helicase loader, but lack DNA helicase functions [11]. Among non-lactococcal phages, those with detectable replicative DNA helicase genes predominantly belong to the family 4 type helicases, also known as superfamily 4 (SF4) helicases [11,16]. Other less represented helicases include homologs of the phage P4 multifunctional primase-helicase protein α, often found alongside superfamily 2 (SF2) helicases, or SF1 Dda-like helicases specific to T4-like phages [17–19].

Helicases are crucial for DNA replication, recombination, and repair, and are categorized into six superfamilies (SF1–6) [16]. These enzymes use the energy from nucleotide triphosphate (NTP) or deoxynucleotide triphosphate (dNTP) hydrolysis to unwind nucleic acid strands [20]. SF4-type helicases, which are hexameric and act at replication forks with 5′ to 3′ translocation activity, are found in both bacteria and phages [16]. The prototype SF4-type helicase is DnaB in *E. coli*, and DnaB-like proteins are present in other bacteria, phages, and mitochondria [21–23]. The best examined phage DnaB-like helicases are the Gp4 primase-helicase of phage T7 and the Gp41 DNA helicase of phage T4 [24–26]. Both helicases are hexameric with a ring-like structure, and unwind DNA in the 5′ to 3′ direction using energy from either dTTP (T7 Gp4) or ATP (T4 Gp41) hydrolysis [27–30].

Each of the six helicase superfamilies is defined by specific sequence motifs. SF4 helicases have five distinct motifs (H1, H1a, H2, H3, and H4) [16], with H1 and H2 corresponding to Walker A (or P-loop) and Walker B motifs, which together with H1a are involved in NTP/dNTP binding and hydrolysis. Motifs H3 and H4 are unique to SF4 helicases and are engaged respectively, in linking NTP hydrolysis with nucleic acid translocation, and in oligonucleotide binding [31]. Together H1-H4 form the active center of the protein [32]. Each of these motifs contains conserved amino acid residues, and biochemical and structural studies on model SF4 helicases (T7 Gp4, plasmid RSF1010 RepA) have detailed their roles in helicase function [33–36].

Previous genome analysis of the *Ceduovirus* phage bIL67 indicated that the early gene (*orf3*) encodes a putative replication protein, likely a polymerase subunit [37]. In this study, we present experimental evidence that a bIL67 ORF3 homolog, the early gene product of the dairy *L. lactis Ceduovirus* bacteriophage 94p4, designated Gp21, is a DNA helicase. Comparative analysis reveals that the 34-kDa Gp21 protein possesses conserved sequence motifs typical of SF4 helicases. We show that Gp21 binds to DNA and unwinds heteroduplex DNA with single-stranded overhangs in a 5′ to 3′ direction, preferably in the presence of ATP and magnesium ions. Substitutions of conserved amino acids within these motifs and subsequent *in vitro* analyses of mutant protein variants indicate that the functional Gp21 protein acts predominantly as a hexamer. The distinctive 5′ to 3′ unwinding activity of Gp21 on branched substrates, coupled with its structural similarity to SF4 helicases, implies its role in phage DNA replication and identifies it as the first functionally confirmed SF4 helicase in *L. lactis Ceduovirus* phages.

2. Materials & methods

2.1. Bioinformatic analysis

To identify homologs of the Gp21 protein from *L. lactis* phage 94p4, a BLAST search was run against the UniProtKB reference proteomes and the Swiss-Prot database [38]. Functional domain searches were performed using the Conserved Domain Database (CDD) implemented in the National Center for Biotechnology Information platform [39] and HMMSCAN 3.4 [40]. Remote homology search was run using HHpred [41]. Modelling of Gp21 quaternary structure was done using AlphaFold3 (accessed on-line) [42]. Multiple sequence alignments of Gp21 with SF4-like helicases were obtained by using MAFFT (localpair, 1000 iterations) [43]. Two-dimensional sequence clustering was made using the CLANS (Clustering Locus-specific ANnotationS) tool [44].

2.2. Bacteriophage, bacterial strains, and growth conditions

E. coli ER2566 strain (New England BioLabs, USA) was cultured at 37 °C with shaking in liquid Luria-Bertani (LB) medium or on LB agar plates (1.5 % agar *w/v*). Ampicillin (Amp; 100 μg mL^{-1}) was added to the medium when required. *L. lactis* bacteriophage 94p4 (full name: vB_Llc_bIBB94p4; GenBank accession no. MH779521) was propagated on *L. lactis* ssp. *cremoris* (currently: *L. cremoris*) strain MG1363 [45] in liquid GM17 medium supplemented with 10 mM calcium chloride as previously described [5].

2.3. Cloning of the gp21 gene

The *gp21* gene was amplified by PCR using primers $gp21_{94p4}$_for and $gp21_{94p4}$_rev (Supplementary File S1) with the phage 94p4 lysate as template. Primers were designed with 5′ modifications to introduce *Sap*I (forward) and *Pst*I (reverse) restriction sites. The amplified DNA fragment was cut and ligated as an N-terminal fusion to the intein-chitin-binding domain (CBD) tag into the pTYB21 vector (New England BioLabs, USA), previously digested by the same enzymes. The recombinant construct was introduced into *E. coli* ER2566 cells by electroporation [46]. Transformants were selected on LB agar plates containing Amp. Colony PCR with pTYB21_F and pTYB21_R primers was used to confirm the presence of the *gp21* insert, and the correctness of the cloned DNA fragment was verified by sequencing.

2.4. Overproduction and purification of the Gp21 protein

Overexpression of the *gp21* gene and subsequent protein purification was carried out using the IMPACT™ Kit system as described by the producer (New England BioLabs, USA). *E. coli* ER2566 cells carrying pTYB21:*gp21* were cultured in 1 L of LB medium supplemented with Amp at 28 °C with shaking until an OD_{600} of ~0.7 was reached. Protein overproduction was induced by adding isopropyl β-D-1-thio-galactopyranoside to a final concentration of 0.4 mM, followed by overnight incubation at 15 °C with shaking. Cells were collected by centrifugation (4 °C, 7000 rpm, 15 min), resuspended in 30 mL of chitin column buffer (50 mM Tris-HCl pH 8, 500 mM NaCl, 10 mM $MgCl_2$) and disrupted by sonication on ice (amplitude 16, for 5 min, with 15-s sonication intervals). The lysate was clarified by centrifugation (4 °C, 11000 rpm, 30 min), and the supernatant was loaded onto a column pre-packed with 10 mL of chitin resin, pre-washed with 100 mL chitin column buffer. The loaded resin was rinsed with 200 mL of chitin column buffer, and the target protein was cleaved from the intein-CBD tag after a 40-h incubation at 23 °C in chitin column buffer containing 50 mM DTT. The eluted protein was analyzed by sodium dodecyl sulfate–polyacrylamide gel electrophoresis (SDS-PAGE). Protein concentration was measured using the Bradford method [47].

2.5. Site-directed mutagenesis of Gp21

Site-directed mutagenesis of Gp21 was performed using the QuikChange II Site-Directed Mutagenesis Kit (Stratagene, USA) with pTYB21:*gp21* as template. Primers (Supplementary File S1) were designed to introduce point mutations substituting amino acids: lysine (K) 48, glutamic acid (E) 81, aspartic acid (D) 135, and histidine (H) 177, with alanine (A). Mutations were confirmed by sequencing the resultant recombinant vectors (pTYB21:*gp21*/K48A, pTYB21:*gp21*/E81A, pTYB21:*gp21*/D135A, pTYB21:*gp21*/H177A). Mutant proteins were overproduced and purified following the same protocol as for the wild-type Gp21 protein.

2.6. Ion exchange chromatography of Gp21 and mutant proteins

Further purification and concentration of wild-type Gp21 and its mutant variants were achieved using ion-exchange chromatography (IEC) on a HiTrap™ Q XL 1 mL column (Cytiva, USA) with the ÄKTA Purifier system (GE Healthcare, USA). The column was equilibrated with a Q column buffer (50 mM Tris-HCl pH 8) with 100 mM NaCl. Protein samples were loaded, and elution was performed with a linear gradient of NaCl (100 mM – 1 M) in the Q column buffer. Eluted protein fractions were analyzed by SDS-PAGE. Protein samples were stored at −20 °C in 50 % glycerol (*v/v*) prior to further experiments.

2.7. Electrophoretic mobility-shift assay (EMSA)

The DNA binding capacity of the wild-type Gp21 protein and its mutant variants was assessed using EMSA. Fluorescently labeled DNA substrates were synthesized in the DNA Sequencing and Synthesis Facility (IBB PAS, Poland) and included single-stranded (ss) oligonucleotides of 45 nt, 68 nt, and 110 nt, 110-bp blunt dsDNA (ds110) generated by PCR using ori110_F and ori110_R primers (Supplementary File S1) with *L. lactis* prolate phage c2 lysate as template, and a branched substrate (30duplex5') generated as described for the helicase DNA unwinding assay. EMSA reactions (20 μL) contained the Gp21 protein at specified concentration, binding buffer (20 mM Tris–HCl pH 8, 50 mM NaCl, 1 mM DTT, 1 mM EDTA, 2.5 % glycerol), 1.5 nM of Cy5-labeled DNA substrates, Milli-Q water and when indicated ATPγS (5 mM). Reactions were incubated at 30 °C for 30 min and analyzed on pre-run 7 % polyacrylamide gels for 20–40 min at 100 V in 0.5× Tris-borate-EDTA (TBE) buffer. Results were visualized on gels using FluorChemQ MultiImageIII ChemiImager (Alpha Innotech, USA) or UVItec Q4 Alliance Unit 3.05 (UVItech, UK) and quantified using ImageJ (Image Processing and Analyzing In Java). The percentage of bound DNA was plotted against protein concentration using nonlinear regression with the "specific binding with Hill slope" model by GraphPad Prism software and the dissociation constants (*Kd*), indicating the protein concentration required to bind half of the DNA substrate and the Hill coefficients (h), which reflect the degree of cooperativity in binding or activity, were calculated for each substrate (Supplementary File S2). All experiments were performed in at least three replicates.

2.8. DNA substrates for helicase DNA unwinding assay

Asymmetric and branched DNA substrates were prepared following the method described by Curti et al. [48] using Cy5-labeled oligonucleotides (Supplementary File S1). Asymmetric heteroduplex DNA substrates, each with a 22-bp dsDNA region and either a 5′ (asym5') or 3′ (asym3') ssDNA overhang, were generated using as5'F/as5'R or as3'F/as3'R primer pairs, respectively. Branched DNA substrates composed of a 30-bp dsDNA segment with two ssDNA overhangs were created using dplx5'F/dplx5'R for a 35-nt 5′ and 15-nt 3′ ssDNA tail (30duplex5') or dplx3'F/dplx3'R for the reverse configuration (30duplex3'). A branched substrate with a 53-bp dsDNA core and a 35-nt 5′ and 15-nt 3′ ssDNA tail (53duplex5') was assembled using the oligonucleotide pair 53dplx5'F/53dplx5'R.

2.9. Helicase DNA unwinding assay

Helicase activity of the wild-type Gp21 protein and its mutant variants was tested using a DNA unwinding assay. The reaction mixture (20 μL) contained the tested protein at given concentration, reaction buffer (20 mM Tris-HCl pH 8, 5 mM $MgCl_2$, 50 mM NaCl), ATP (at given concentration, unless the use of other NTPs, dNTPs or ATPγS was indicated), 1.5 nM Cy5-labeled DNA substrate, and Milli-Q water. The reaction was incubated at 30 °C for 30 min and then stopped by adding 6 μL of stop solution (10 % glycerol, 0.4 % SDS, 50 mM EDTA). To minimize reannealing of the unwound oligonucleotides, a 10-fold molar excess of unlabeled DNA trap, corresponding to the Cy5-labeled strand was added after 10 min of the reaction. The DNA substrate denatured by heating for 30 min at 100 °C served as an indicator of successful DNA unwinding. Samples were analyzed on a pre-run 15 % polyacrylamide gel for 20–40 min at 100 V in 0.5× TBE buffer. The results were visualized using the FluorChemQ MultiImageIII ChemiImager (Alpha Innotech, USA) or the UVItec Q4 Alliance Unit 3.05 (UVItec, UK) and quantified using ImageJ software (Image Processing and Analyzing In Java). The percentage of unwound DNA was plotted against protein concentration using three-parameter nonlinear regression model ([agonist] *vs.* response) with GraphPad Prism software and half-maximal effective concentration (EC_{50}), representing the protein concentration at which DNA unwinding reaches half of its maximum, was calculated for each substrate (Supplementary File S3). All experiments were performed in at least three replicates.

2.10. Size exclusion chromatography with multi-angle light scattering (SEC-MALS) analysis

SEC-MALS analysis was performed using a high-performance liquid chromatography (HPLC) system equipped with a Binary HPLC Pump 1525 and a UV/VIS Detector 2489 (Waters, USA), along with two detectors: Dawn 8+ multi-angle MALS detector and Optilab T-rEX refractive index detector (Wyatt Technology, USA). Protein samples (1.4 mg mL^{-1}) were loaded onto an XBridge BEH-200A SEC column (Waters, USA) and run at room temperature with a flow rate 1 mL min^{-1} in a buffer containing 50 mM Tris-HCl pH 8 and 300 mM NaCl.

2.11. CD spectroscopy

Circular dichroism (CD) spectra were acquired using a Jasco J-815 CD spectropolarimeter (Jasco Int. Co., Ltd., Japan) at a temperature of 25 °C. Measurements were performed in a quartz cuvette with a path length of 0.02 cm, covering the spectral range of 185–260 nm. Protein samples were prepared at a concentration of 5 μM. Spectral data were recorded in 25 mM NaF solvent condition at 0.5 nm intervals, with each sample undergoing four consecutive scans, which were subsequently averaged. The bandwidth was maintained at 1.0 nm. To correct for background signals, the baseline spectrum of the solvent was subtracted from the protein spectra. To express the CD data in standard units, the raw values recorded in millidegrees (mdeg) were converted to molar ellipticity (θ) with units of deg·cm^2·$dmol^{-1}$ (Supplementary File S4). This transformation was performed using standard calculations, taking into account the peptide concentration and the path length of the cuvette. To minimize noise while preserving the inherent spectral features, we applied the Savitzky-Golay (SG) filter to the raw CD data. Specifically, the filter was implemented using the savgol_filter function in Python's scipy.signal library [49]. The SG method fits a local polynomial of a specified order across a moving window of the data. We employed a window length of 111 data points and a polynomial order of 8, based on preliminary tests that compared various parameter sets (window lengths: 7, 9, 11, 81, 101, 111, 121; polynomial orders: 2, 3, 7, 8, 9). This larger window and higher-order polynomial were chosen because they effectively suppressed high-frequency noise while maintaining the overall shape of the broad spectral features present in our measurements (Supplementary Fig. S1). The α-helical content of the protein was estimated based on the ellipticity value at 222 nm (θ_{222nm}) using a standard calculation formula [50].

3. Results

3.1. In silico identification of Gp21 homologs

The *gp21* gene of the prolate-headed *L. lactis* phage 94p4, located in the early gene region of the phage genome, shows high homology (97 % identity) to *orf3* of the model lactococcal phage bIL67, annotated as

encoding a DNA polymerase subunit [37]. However, the function of this gene has never been experimentally confirmed. All fully sequenced prolate-headed lactococcal phage genomes available in GenBank (as of December 2024) carry a well-conserved homolog (> 90 % identity) of the *gp21* gene product (Gp21), indicating its potential importance in the phage life cycle. CDD analysis identified a RecA-like NTPase domain within Gp21, though it lacks primary sequence similarity to NTPases of known function. A search against the UniProtKB reference proteomes and Swiss-Prot database returned several hits, mainly to proteins annotated as putative DNA polymerases. Among the identified matches was a hypothetical protein from the gram-negative bacteria *Oceanibaculum pacificum* (AUP43_16330) containing an SF4 helicase domain and showing 46.1 % sequence similarity. According to the pfam database, Gp21 is classified to the AAA_25 family (PF13481), and based on pairwise sequence comparisons it clusters together with RepA-like proteins. As visualized by the CLANS analysis, Gp21, together with multiple phage homologs, remains at the border of the RepA cluster, forming a distinct group from the DnaB-like SF4 helicases, which might suggest its evolutionary divergence (Fig. 1). Using HHpred for remote homology searches and structural predictions, Gp21 was found to share high structural similarity with known SF4 helicases, including Gp4 from *E. coli* phage T7 (probability: 99.75 %, e-value: 2.8e-16), Gp41 helicase/primase from phage T4 (probability: 99.73 %; e-value: 2.9e-15), G40P from *Bacillus subtilis* phage SPP1 (probability: 99.72 %, e-value: 2.5e-15), and RepA helicase from *E. coli* plasmid RSF1010 (probability: 99.86 %, e-value: 8.2.e-20) – all involved in DNA replication. Multiple sequence alignments identified key motifs characteristic of SF4 helicases, including H1 (Walker A), H2 (Walker B), and motifs H1a, H3 and H4, each containing conserved amino acids (Fig. 2A). *In silico* modelling showed that Gp21 adopts essentially a similar fold as RepA of the RSF1010 plasmid and the T7 Gp4 helicase and indicated the position of the motif regions and conserved residues within them (Fig. 2B).

3.2. DNA binding activity of Gp21

The purified Gp21 protein (Supplementary Fig. S2) was assessed for

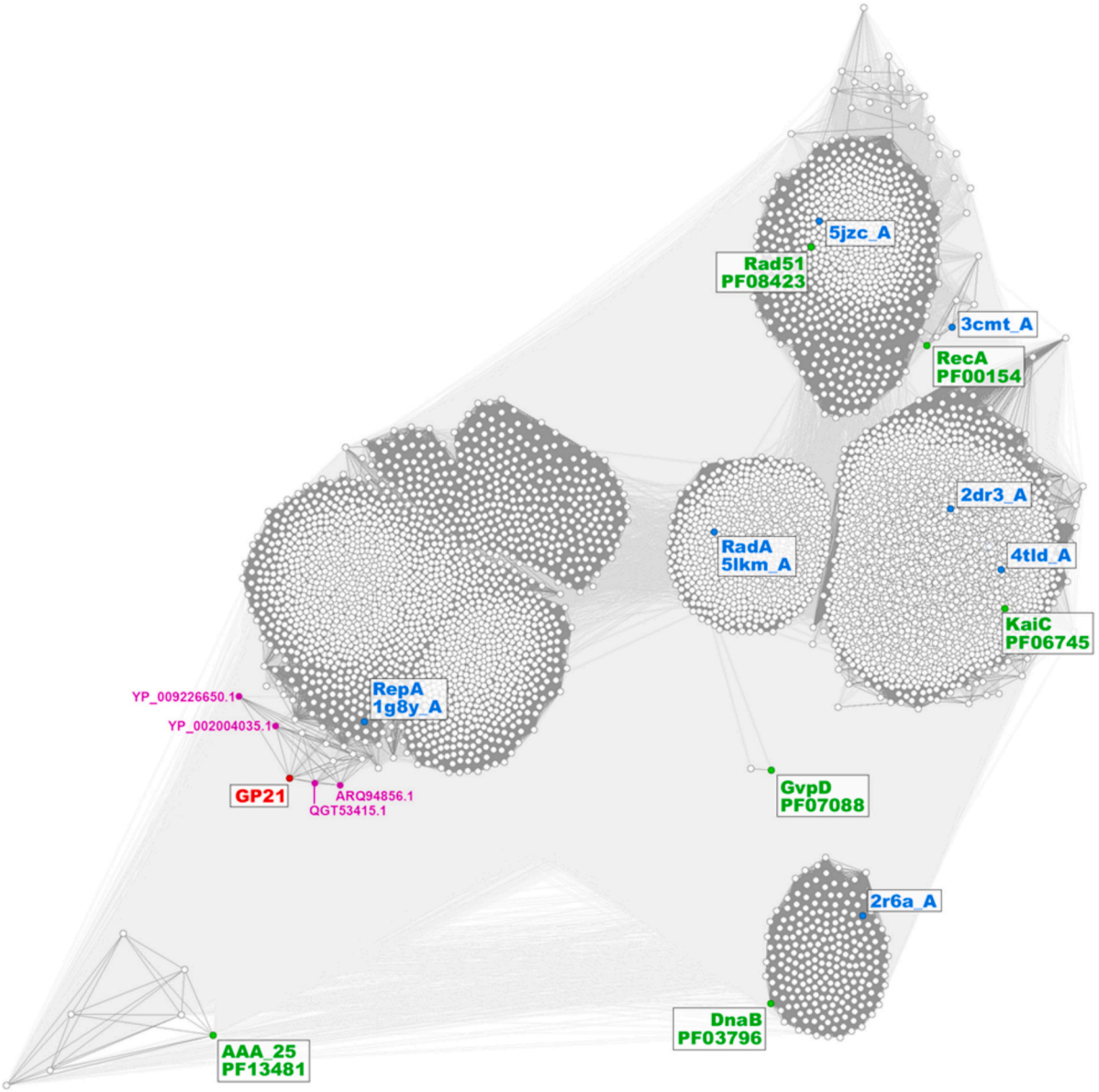

Fig. 1. Clustering of SF4 helicases, including Gp21 of *L. lactis* phage 94p4, and other NTPase protein families. Dots mark protein sequences; in green: consensus sequence for a given family; in blue: proteins with known structures; in pink phage proteins in the immediate neighborhood of Gp21 (in red). Similarities between protein sequences are marked with grey lines of varying shades: light grey (*P*-value <0.001), medium grey (P-value <1E-20) and dark grey (P-value <1E-30).

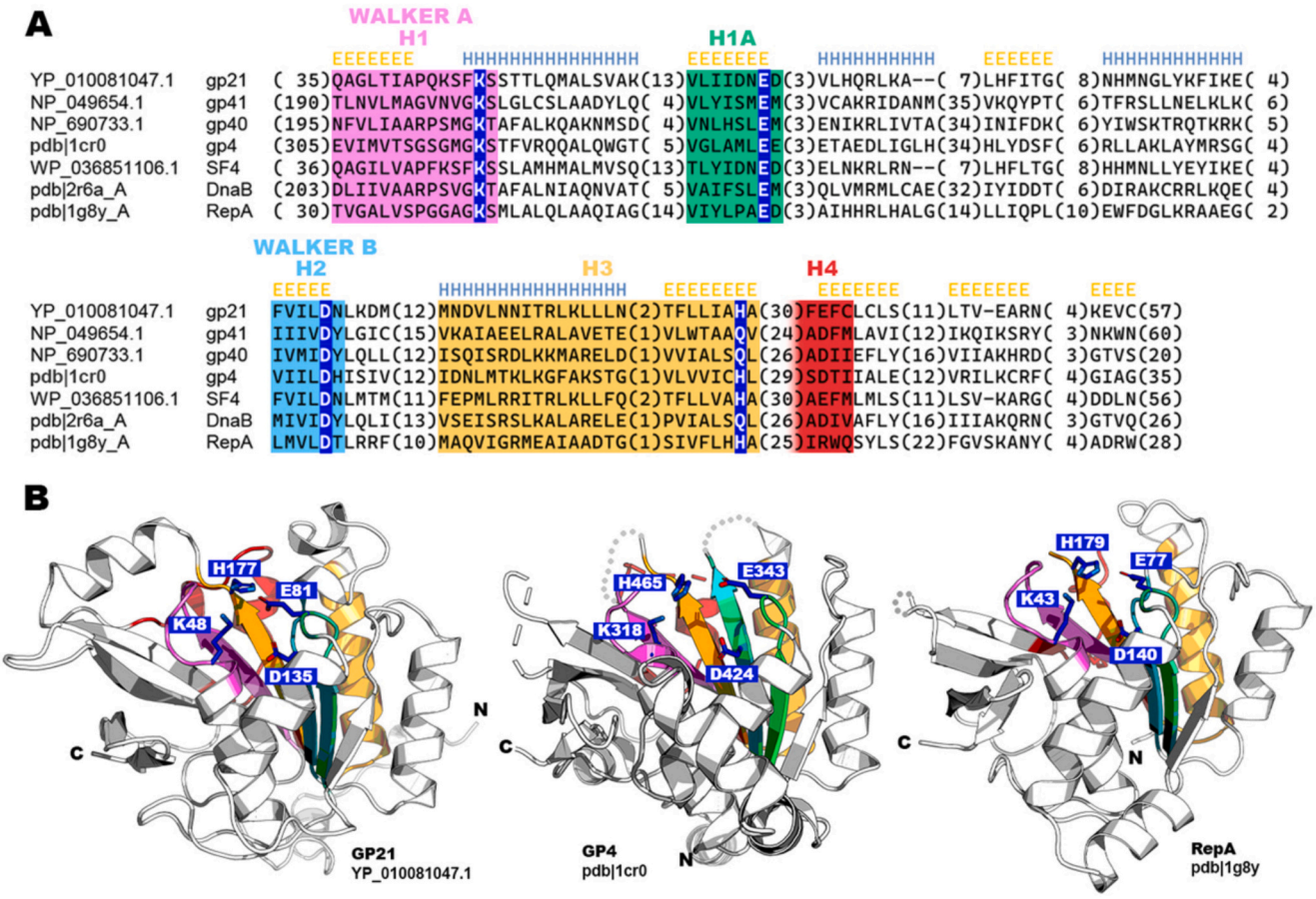

Fig. 2. Comparative sequence and 3-D structure model analysis of Gp21 with SF4 helicases.
(A) Multiple sequence alignment of Gp21 with known SF4 helicases; sequence coordinates are based on GenBank accession numbers, UniProt ID, or PDB codes. Values in parentheses indicate the number of residues excluded from the alignment. Secondary structure elements are shown above the alignment: 'EEE' represents ß-strands and 'HHH' denotes α-helices. (B) *In silico* 3-D model of wild-type Gp21 protein and structural comparison with the SF4-type Gp4 protein of phage T7 and RepA protein of RSF1010 plasmid. Motifs are colour-coded: H1 (Walker A) in pink, H1a in green, H2 (Walker B) in blue, H3 in yellow, and H4 in red – with conserved amino acids highlighted on a navy blue background.

its affinity to DNA using EMSA with a range of DNA substrates (Fig. 3). Fixed amounts of DNA were incubated with increasing concentrations of Gp21 under non-denaturing conditions specifically designed to preserve nucleoprotein complexes. DNA binding was evaluated by the appearance of shifted bands in the gel, indicating the formation of stable DNA-Gp21 complexes. Gp21 displayed variable binding to ssDNA (Fig. 3A-C), with increasing affinity correlating with substrate length. The weakest interaction was observed with ss45 (*Kd* of 0.82 μM), while binding was stronger for ss68 (*Kd* 0.49 μM) and most efficient for ss110 (*Kd* 0.42 μM) with >90 % shift at 0.75 μM concentration (Fig. 3F, Table 1). All ssDNA substrates showed Hill coefficients >2 indicating cooperative binding, which increased on longer oligonucleotides potentially due to the formation (or stabilization) of oligomeric complexes (Table 1). In contrast, no binding was observed with ds110 indicating that Gp21 requires single-stranded regions for stable interaction and cannot efficiently engage blunt-ended dsDNA (Fig. 3D & F). Given the structural similarity of Gp21 to SF4 replicative DNA helicases, its binding affinity for a branched substrate mimicking replication forks (30duplex5') was also tested (Fig. 3E). This substrate was most efficiently bound among all DNA types (*Kd* 0.32 μM), indicating that structured (duplex) substrates enhance Gp21 loading onto ssDNA through stabilization of the complex or a preferred loading configuration (Fig. 3F, Table 1). The presence of a non-hydrolyzable ATP analog (ATPγS) in the EMSA reaction mixture decreased the affinity of Gp21 for DNA, suggesting that in its ATP-bound state, the protein interacts with DNA more transiently and exhibits an increased tendency to dissociate (Supplementary Fig. S3). Additionally, with ssDNA, high molecular weight (HMW) aggregates were observed, indicated by DNA retained in the wells (Fig. 3A-C) not seen with dsDNA or branched substrates (Fig. 3D and E). This might suggest strong interaction of Gp21 with ssDNA, resulting in large HMW aggregates that do not migrate into the gel.

3.3. Helicase activity of Gp21

To validate the predicted helicase activity of Gp21, we performed DNA unwinding assays using a variety of cofactors and substrates. To improve the resolution of reaction products during native gel electrophoresis, specific competitor DNA was added to stabilize the unwound structures and an SDS-containing stop buffer was used to quench the reaction and displace Gp21 from the DNA.

3.3.1. Cofactor-dependent unwinding activity of Gp21

The optimal reaction requirements for Gp21 helicase activity were determined using branched DNA substrate mimicking replication forks (30duplex5') and varying ATP concentrations (0–15 mM) at a constant Mg^{2+} level (5 mM). DNA unwinding was equally efficient in a 5–10 mM ATP concentration range, corresponding to ATP:Mg^{2+} 1–2 ratio (Fig. 4A-B). Alternatively, no activity was detected in reactions conducted in the absence of ATP or containing ATPγS, confirming that hydrolysis of the nucleotide cofactor is required for Gp21-driven DNA unwinding (Supplementary Fig. S4). We established that the lack of DNA unwinding was not due to Gp21 inability to bind ATPγS, as adding ATP

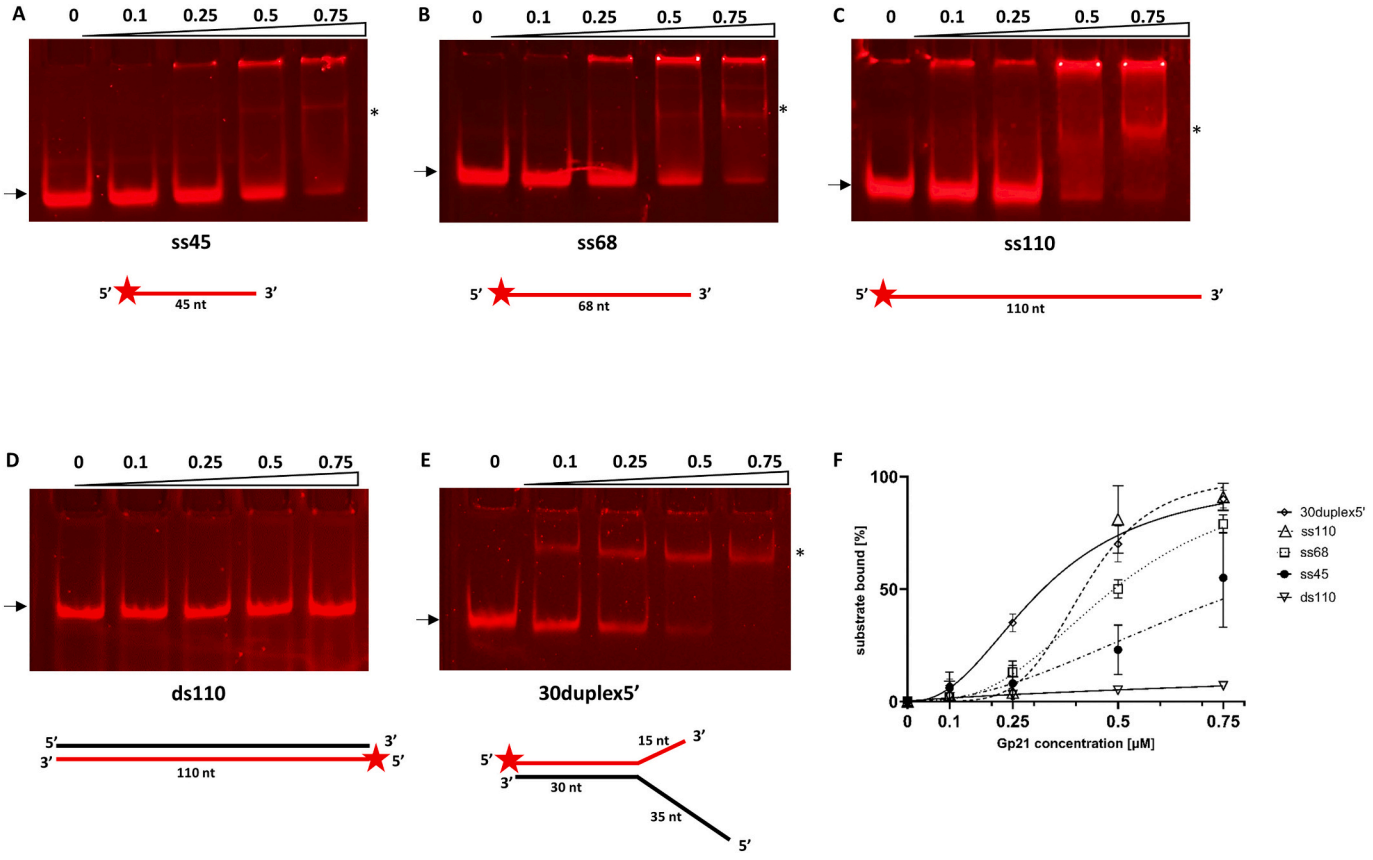

Fig. 3. EMSA assay of Gp21 DNA binding activity.
Increasing concentrations of Gp21 protein (μM) were incubated as described in Materials & methods with a fixed amount (1.5 nM) of Cy5-labeled oligonucleotides: (A) 45-mer, (B) 68-mer, (C) 110-mer, (D) 110-bp dsDNA (ds110), or (E) branched substrate (30duplex5'). Nucleoprotein complexes with reduced mobility are marked by asterisks (*); arrows indicate the migration position of the free DNA substrates. The red star on substrate diagrams represents Cy5 labeling. (F) Quantitative assessment of Gp21 DNA binding activity as a function of protein concentration on various DNA substrates. Data represent the average of three independent experiments with standard deviations (SD) indicated by error bars.

Table 1
Apparent dissociation constant (*Kd*) and Hill coefficient (h) of Gp21 concentration-dependent binding to DNA.

Parameters	DNA substrates				
	ss45	ss68	ss110	ds110	30duplex5'
h	2.1	2.9	5.2	n.d.	2.4
Kd [μM]	0.82	0.49	0.42	n.d.	0.32
R^{2*}	0.94	1	1	n.d.	1

* R^2: proportion of variance in the dependent variable explained by the model (0–1 scale).

to reactions initiated with ATPγS did not restore helicase activity. Conversely, ATPγS addition inhibited unwinding in reactions started with ATP (Supplementary Fig. S5). Also in reactions lacking Mg^{2+} ions, no DNA strand separation was detected, highlighting the critical role of both ATP and Mg^{2+} in supporting helicase activity (Fig. 4A). At 15 mM ATP, a drop in the unwinding level was noted. Based on these results, we adopted a 1:1 ATP:Mg^{2+} ratio as the standard condition for all further assays. Substituting ATP with other NTPs or dNTPs in the reaction mixture led to reduced unwinding efficiency, indicating preference for ATP as a nucleotide cofactor (Supplementary Fig. S6).

3.3.2. *Gp21 unwinds DNA substrates in a 5′ to 3′ direction*

To determine the unwinding polarity of Gp21, we used asymmetric DNA substrates containing either a free 5′ (asym5') or a 3′ (asym3') ssDNA end. Gp21 showed limited unwinding of the 5′-tailed substrate, reaching only 35 % strand separation at 1 μM protein concentration, with half-maximal effective concentration (EC_{50}) of 2.39 μM (Fig. 5A & F, Table 2). No unwinding was observed for the 3′-tailed substrate, even at the highest tested concentrations (Fig. 5B & F). These findings indicate that Gp21 displays helicase activity with a 5′ to 3′ unwinding direction, albeit acting weakly on asymmetric substrates.

3.3.3. *Gp21 unwinding activity on fork-like substrates*

We further investigated the Gp21 preference to unwind replication fork-like DNA structures using two synthetic branched substrates with 5′ ssDNA tails of varied lengths: 35 nt in 30duplex5' and 15 nt in 30duplex3', across a gradient of rising Gp21 concentrations. Gp21 was active on both substrates, with unwinding observed from 0.2 μM concentration (Fig. 5C-D). The 30duplex5' was unwound more efficiently, with apparent EC_{50} of 0.2 μM and 95 % strand separation at 1 μM, compared to EC_{50} of 0.34 μM and 78 % unwinding of the 30duplex3' at the same protein concentration (Fig. 5F, Table 2). A longer duplex substrate (53duplex5') was also unwound, but with a reduced efficiency (66 % at 1 μM) and a higher EC_{50} (0.48 μM) (Fig. 5E-F, Table 2). These findings indicate that Gp21 initiates unwinding preferentially on branched over asymmetric substrates, requiring 5′ ssDNA overhangs of at least 15 nt.

3.4. *Gp21 forms hexamers in solution*

The oligomeric state of the native Gp21 protein in solution was examined using SEC-MALS. The results revealed that Gp21 self-

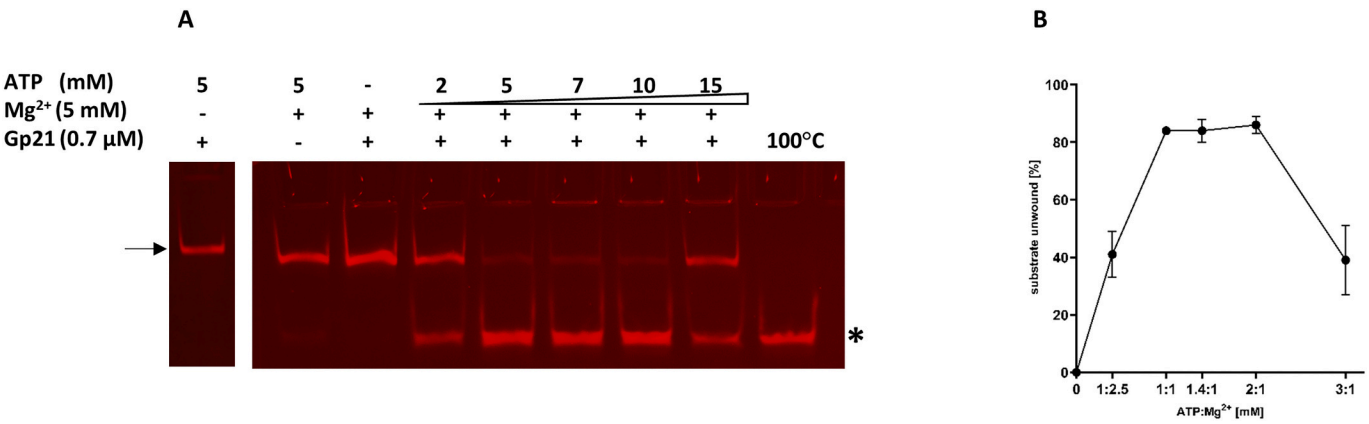

Fig. 4. ATP and Mg^{2+} as cofactors of the Gp21 DNA unwinding activity.
(A) Reactions were performed as described in Materials & methods using 1.5 nM Cy5-labeled 30duplex5', 5 mM $MgCl_2$ and increasing concentrations of ATP (0–15 mM). The asterisk (*) marks the expected position of the displaced Cy5-labeled strand based on heat denaturation (100 °C); the arrow indicates the intact substrate position. (B) DNA unwinding as a function of cofactor stoichiometry (ATP:Mg^{2+}). Data represent the average of three independent experiments with standard deviations (SD) indicated by error bars (Supplementary File S5).

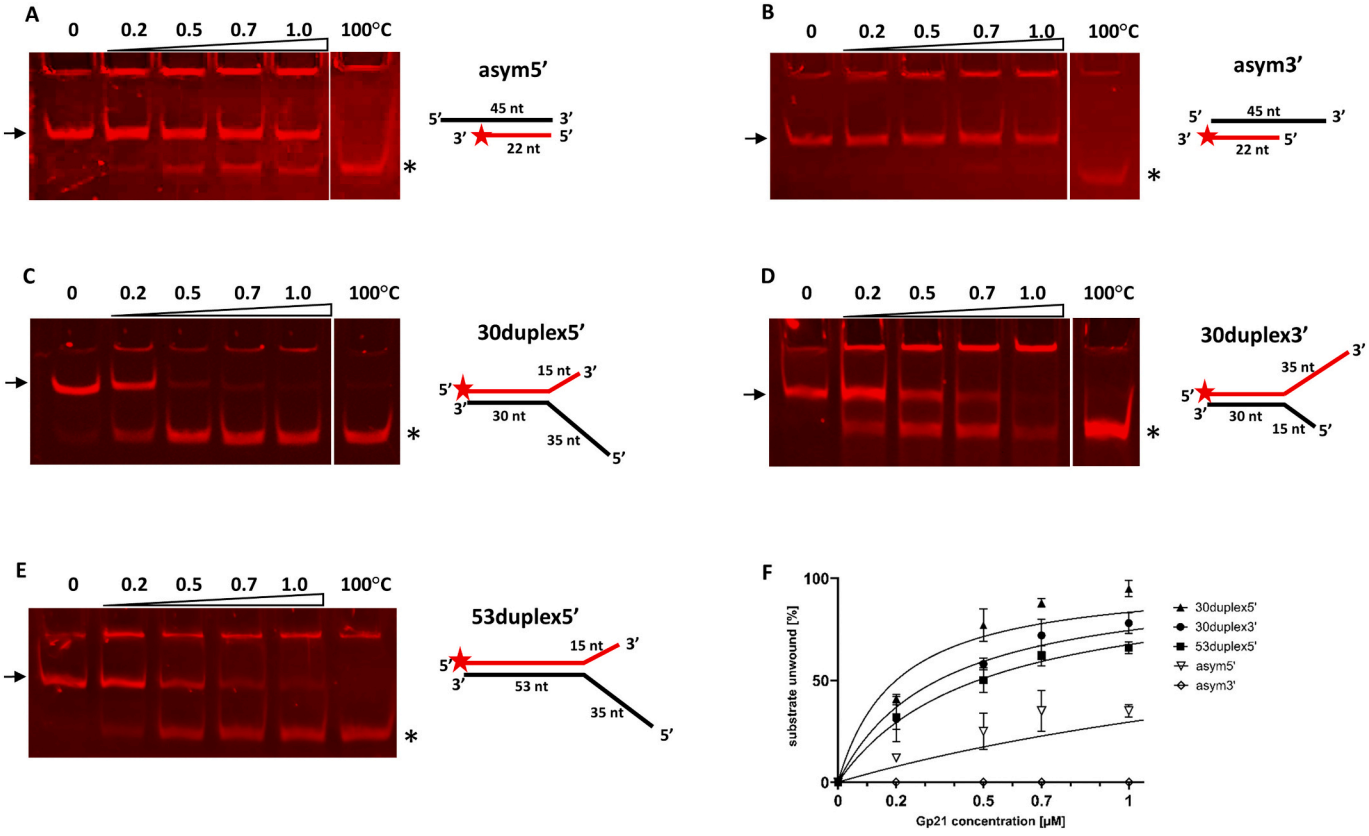

Fig. 5. DNA unwinding activity of Gp21.
Increasing concentrations of Gp21 (µM) were incubated as described in Materials & methods with 1.5 nM Cy5-labeled DNA substrates: (A) asym5', (B) asym3', (C) 30duplex5', (D) 30duplex3', or (E) 53duplex5'. Asterisks (*) mark the expected position of the displaced Cy5-labeled strand based on heat denaturation (100 °C); arrows indicate the intact substrate position. The red star on substrate diagrams represents Cy5 labeling. (F) Quantitative assessment of Gp21 DNA unwinding activity as a function of protein concentration on various DNA substrates. Data represent the average of three independent experiments with standard deviations (SD) indicated by error bars.

associates, forming multiple species, as indicated by its chromatographic profile (Fig. 6A). The majority of the protein eluted as three overlapping peaks with molecular masses corresponding to the theoretical molecular weights of a heptamer, hexamer and pentamer. Other peaks indicated the presence of both a high-order multimer and a 34-kDa monomer.

To test which protein species retained helicase activity, we performed unwinding assays using 30duplex5' on each of the eluted fractions. Only heptameric and hexameric fractions, which eluted respectively at 7.3 min and 8.2 min, demonstrated evident strand displacement activity (Fig. 6B), confirming that the helicase function of Gp21 is associated with these oligomeric states.

Table 2
Half-maximal effective concentrations (EC_{50}) required for Gp21-mediated DNA unwinding of duplex DNA substrates.

Parameters	DNA substrates				
	30duplex3'	53duplex5'	30duplex5'	asym5'	asym3'
EC_{50} [μM]	0.34	0.48	0.20	2.39	n.d.
R^{2*}	1.00	1.00	0.98	0.95	n.d.

* R^2: proportion of variance in the dependent variable explained by the model (0–1 scale).

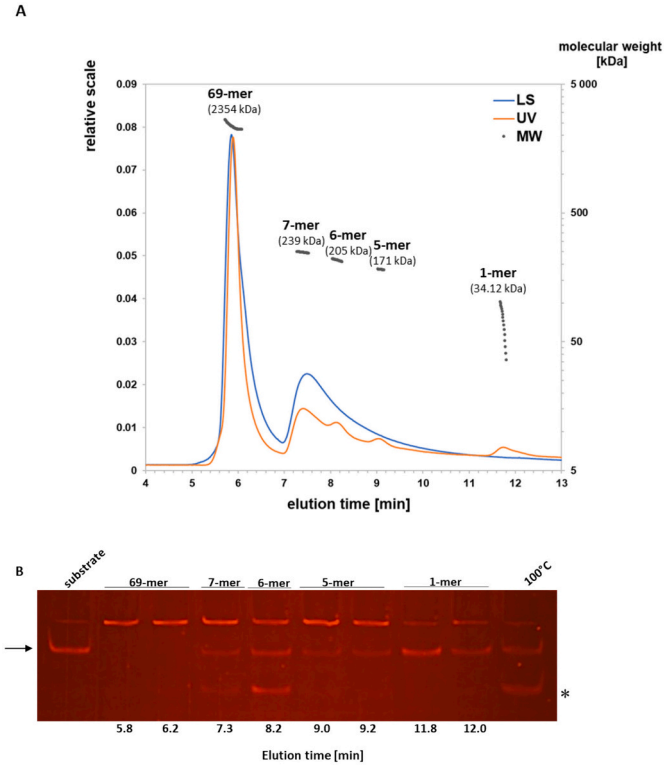

Fig. 6. Analysis of Gp21 multimerization using SEC-MALS.
(A) SEC-MALS elution profile of the Gp21 protein. Left axis shows light scattering (blue) and UV absorbance (orange) on a relative scale, while the right axis indicates the molecular weight of the protein in log scale (short grey lines). Protein oligomeric states are provided at the relevant peaks and were assigned based on peak molecular weight read-outs (in parenthesis).
(B) Helicase activity assay of SEC-MALS-eluted fractions using 30duplex5'. The asterisk (*) marks the expected position of the displaced Cy5-labeled strand based on the heat denaturation (100 °C); the arrow indicates the intact substrate position.

3.5. Functional activity of Gp21 mutant variants

In silico analysis of Gp21 led to the identification of conserved amino acids within motifs characteristic of SF4-type helicases (Fig. 2). To probe their functional significance, we carried out site-directed mutagenesis, substituting lysine 48 (K48) in motif H1, glutamic acid 81 (E81) in motif H1a, aspartic acid 135 (D135) in motif H2, and histidine 177 (H177) in motif H3 with alanine (A). For examining the catalytic importance of the substituted residues, we overproduced and purified the Gp21 mutant variants (Supplementary Fig. S2). To assess whether the secondary structure remained intact following amino acid substitutions and to confirm that the mutant proteins were properly folded, CD spectroscopy was employed. The results indicated that none of the introduced substitutions disrupted the overall structure of the Gp21 protein (Fig. 7). The α-helicity of the mutant variants was preserved within a range

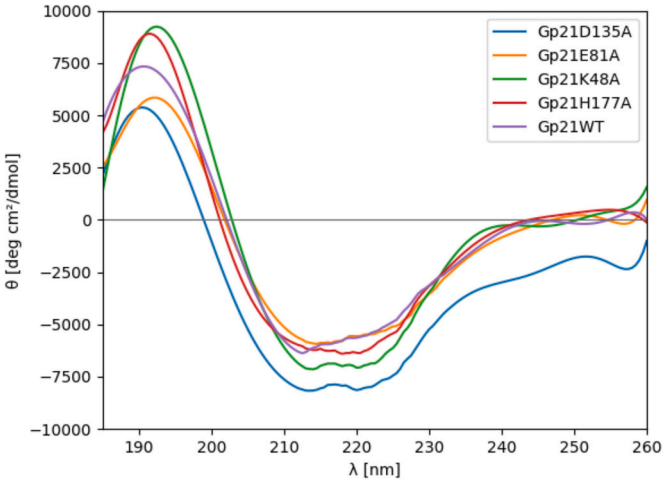

Fig. 7. CD spectra of wild-type Gp21 (GpWT) and its mutant variants (Gp21K48A, Gp21E81A, Gp21D135A, Gp21H177A), expressed in molar ellipticity (θ) with units of deg·cm^2·dmol^{-1}.

comparable to that of the wild-type Gp21 protein (22–28 %), suggesting that the substitutions did not significantly alter its structural integrity. Furthermore, the CD spectra shapes of the mutant proteins largely overlapped well with that of the wild type, with only minor differences observed, particularly in the intensity of ellipticity signals, further confirming structural similarity (Fig. 7, Supplementary Fig. S1). Further on, we evaluated the DNA-binding capacity of the mutant proteins by EMSA assays. The obtained data showed that all of the protein variants, except K48A, retained their affinity for DNA comparable to the wild type, indicating that the introduced amino acid substitutions did not abolish this function (Fig. 8). The notably weaker binding of the K48A mutant suggests a role of this residue in stabilizing the DNA interaction or the DNA binding interface of Gp21. Additionally, similar to the wild-type Gp21, the mutant proteins exhibited weaker affinity for DNA in the presence of ATPγS (Supplementary Fig. S3), suggesting that they likely undergo comparable conformational changes upon cofactor binding.

3.5.1. Conserved residues are essential for Gp21 helicase activity

While the Gp21 mutant variants maintained DNA-binding capacity and the secondary structure like that of the wild-type protein, their DNA helicase activity was completely abolished. Helicase assays using 30duplex5' showed no detectable unwinding by any mutant in the presence of ATP (or ATPγS) (Fig. 9A, Supplementary Fig. S4), indicating that the substituted residues are essential for catalytic helicase function

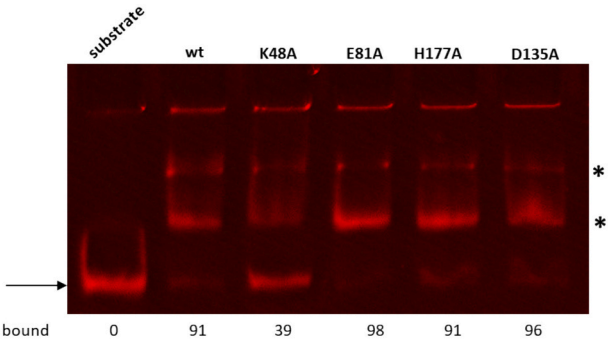

Fig. 8. EMSA assay of DNA-binding activity of Gp21 mutant variants.
Proteins (0.7 μM) were incubated as described in Materials & methods with 1.5 nM Cy5-labeled 30duplex5'. Nucleoprotein complexes with reduced mobility are marked by asterisks (*); the arrow indicates the migration position of the free DNA substrate. Values underneath the images present the % of bound DNA based on measurements of the DNA band intensities visualized on the gel.

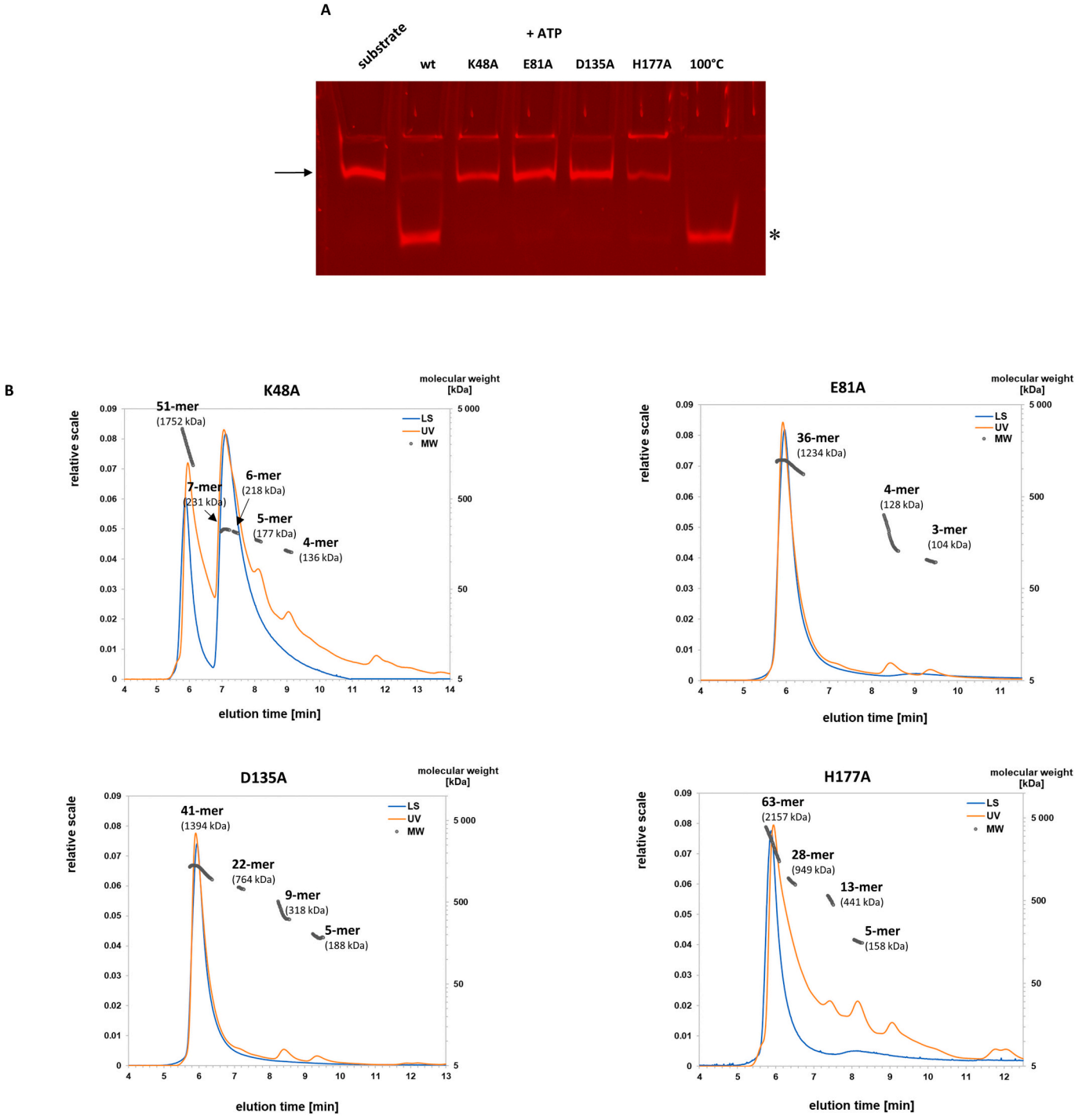

Fig. 9. Helicase activity and multimerization analysis of Gp21 mutant variants.
(A) Proteins (0.7 μM) were incubated as described in Materials & methods with 1.5 nM Cy5-labeled 30duplex5'. Asterisk (*) marks the position of the displaced strand based on the heat denaturation (100 °C); the arrow indicates the intact substrate position. (B) SEC-MALS elution profiles of Gp21 mutants. Left axis shows light scattering (blue) and UV absorbance (orange) in relative scale, and the right axis shows the molecular weight of the protein in log scale (short grey lines). Protein oligomeric states are provided at the relevant peaks and were assigned based on peak molecular weight read-outs (in parenthesis).

rather than for DNA binding itself.

3.5.2. *Multimerization of Gp21 mutant variants*

To investigate the lack of helicase activity of the Gp21 mutant variants, we used SEC-MALS to examine their multimerization ability, which is essential for DNA unwinding. While the wild-type Gp21 predominantly formed hexamers and heptamers (Fig. 6A), the mutants displayed distinct elution profiles. Among the variants, only K48A retained the capacity to form hexamers and heptamers, with a shift toward the heptameric fraction. The other mutant variants (E81A, D135A, and H177A) predominantly eluted as high-order multimers, with faint signals corresponding to smaller oligomers, indicating possible oligomer dissociation (Fig. 9B). Collectively, these results suggest that residues E81, D135, and H177 are critical for maintaining both the multimerization profile and helicase activity of Gp21. In contrast, K48 is essential for helicase function but does not fully abolish the protein's

ability to hexamerize.

4. Discussion

This study elucidates the function of Gp21, an early-expressed gene product of the lytic *Ceduovirus* phage 94p4, isolated from *L. lactis* in a Polish dairy plant [5]. Initially, based on sequence similarity to the *L. lactis* phage bIL67 ORF3, annotated as a DNA polymerase subunit [37], Gp21 was assumed to play an analogous role. However, subsequent *in silico* studies classified Gp21 as a member of the RecA-like NTPase superfamily [5], which groups functionally diverse proteins that couple NTP hydrolysis to essential cellular processes [51]. Given the prevalence of NTPase domains in approximately 5–10 % of predicted gene products across both eukaryotes and prokaryotes [52], we employed *in vitro* and *in silico* approaches to clarify the role of Gp21 in phage replication.

Our functional assays demonstrate that Gp21 binds ssDNA cooperatively, with binding affinity increasing with oligonucleotide length. Similar cooperative behavior has been observed in other SF4 helicases, including T7 Gp4, and is thought to be critical for efficient helicase loading at replication forks [20]. Moreover, Gp21 shows no detectable interaction with blunt-ended dsDNA, indicating its strict preference for single-stranded regions. Interestingly, Gp21 dissects asymmetric substrates with a single free 5′ ssDNA tail, consistent with 5′ to 3′ unwinding polarity. Activity on such substrates is accordant with the RSF1010 RepA helicase, although it is relatively rare among SF4 helicases [53]. Unlike RepA, which shows peak activity at pH 5.5–6, Gp21 is most active in pH 8. Weak unwinding on asym5' substrates suggests that a 5′ tail alone is insufficient for efficient strand separation. The strongest binding is observed with a branched DNA substrate mimicking a replication fork, supporting the notion that Gp21 may rely on such architectures for optimal activity *in vivo*. This requirement aligns with most helicases, such as T7 Gp4, T4 Gp41, and *E. coli* DnaB, which require forked DNA with ssDNA overhangs for efficient unwinding [54].

Reduced DNA-binding affinity of Gp21 in the presence of ATPγS seems to reflect the functional behavior of helicases, which cycle between DNA-bound and unbound states during translocation. Similar observations have been reported for other helicases, including SARS-CoV-2 Nsp13 and HCV NS3h, where ATP or its non-hydrolyzable analogs were shown to decrease binding to DNA compared to nucleotide-free conditions [55,56]. In NS3h, reduced affinity for ssDNA in the ATP-bound state has been proposed to facilitate helicase progression, with tighter rebinding occurring after ATP hydrolysis [57]. This ATP-dependent complex destabilization likely reflects a shift from the loading or initiation state to an active unwinding mode, where transient DNA interactions are essential for helicase translocation along the strand. Such a mechanism is consistent with the Brownian model of unidirectional helicase movement. The DNA-binding behavior of Gp21 in the presence *vs.* absence of ATPγS suggests a similar mechanism, although further investigations are required to fully elucidate this process.

Reduced DNA binding under ATPγS conditions is also observed for Gp21 variants bearing substitutions in the H1, H1a, H2 and H3 motifs. Previous studies on other SF4 helicases implicated these motifs in ATP binding and hydrolysis (H1,H2), conformational flexibility for nucleotide processing (H1a), and coordination of subunit dynamics during translocation (H3) [31]. Further insights could be provided by examining a mutant in the H4 motif, which has been linked to ssDNA interaction in SF4 helicases. Such mutant would help determine whether this region directly coordinates the DNA backbone or acts through structural or allosteric stabilization of the DNA-bound conformation of Gp21. Moreover, comparison of wild-type and H4 mutant ssDNA binding in different nucleotide-bound states (*e.g.*, ATPγS, ATP, or none) could clarify how nucleotide binding affects DNA recognition and conformational changes.

Like other RecA-like NTPases with SF4-type helicase activity, Gp21 displays specific cofactor requirements. These requirements vary among SF4-type helicases. RSF1010 RepA utilizes a broad spectrum of NTPs/dNTPs [53], T4 Gp41 requires ATP or GTP [30], while T7 Gp4 helicase prefers dTTP [58]. Gp21 demonstrated robust ATP-dependent DNA unwinding, with other NTPs and dNTPs supporting this activity at lower efficiency, potentially due to reduced binding affinity to Gp21 or decreased turnover rates. No unwinding was detected in the absence of ATP or when it was substituted with ATPγS. Moreover, ATPγS addition inhibited ongoing reactions, indicating that ATP hydrolysis (not only ATP binding) is essential for Gp21 function. Our data also show that helicase activity is sensitive to the ATP:Mg^{2+} ratio, with optimal activity at equimolar concentrations. Inhibition at high ATP levels may result from Mg^{2+} chelation by excess ATP, reducing the catalytically active Mg^{2+} pool. Excess of free ATP may also compete with binding of the ATP:Mg^{2+} complex to the protein, inducing non-productive conformations, as reported for RecQ helicase [59].

SF4-type replicative DNA helicases typically self-assemble into ring-shaped hexamers, forming a central channel that accommodates one DNA strand while displacing the complementary strand during translocation [15,16]. Our *in silico* analysis revealed conserved motifs and structural folds characteristic of this class in Gp21. SEC-MALS analyses confirmed that in its native state, Gp21 forms predominantly hexamers with some pentamers and heptamers. In our experiments, only the hexameric form of wild-type Gp21 was able to unwind branched DNA substrates, suggesting that Gp21 operates *via* a ring-opening mechanism rather than monomeric ring assembly. This model has been proposed for *E. coli* DnaB [60] and T7 Gp4 [61], where preformed rings open transiently to load onto DNA. Although the hexamer appears to be the only functionally active form responsible for DNA unwinding, the coexistence of multiple oligomeric forms suggests a dynamic equilibrium in which hexamers may interconvert with heptamers or pentamers. Similar transitions have been described for other helicases and are often stabilized by cofactors, such as Mg^{2+} (DnaB), dTTP (T7 Gp4), or ATP (T4 Gp41) [62–64]. Although Gp21 hexamerization was observed under nucleotide-free conditions, resembling the RSF1010 RepA helicase [36], we cannot rule out the possibility that a specific cofactor may further stabilize this oligomeric state.

In contrast, Gp21 mutants predominantly formed higher-order oligomers and lacked helicase activity. Since their secondary structure and DNA binding were maintained, we attribute the loss of function to the disruption of mechanistically important residues. Among them, only K48A retained a hexameric form, though its oligomerization profile was shifted toward a heptamer. The K48A residue lies within the H1 (Walker A) motif critical for ATP binding, and its mutation likely disrupts ATPase activity [65]. The K48A variant exhibited also the most pronounced binding defect and may also be impaired in converting from heptamer to hexamer, a transition known to be essential for helicase function in T7 Gp4 [62]. Although ATP binding in this mutant is likely residual, it may still be sufficient to trigger conformational or oligomeric changes. We preliminarily explored the potential influence of ATP on the oligomerization state of all Gp21 mutant variants using dynamic light scattering (DLS) analysis. These data (not shown) indicated that higher-order oligomers remained the dominant species, regardless of the presence or absence of ATP. While DLS may have limitations in discerning subtle changes within a heterogeneous population of large oligomers, this initial assessment did not reveal a significant shift in their overall size distribution. A more detailed exploration of the role of ATP in the precise dynamics of oligomerization, employing complementary techniques, would be a valuable avenue for future research.

Although *Ceduovirus* phages seem to rely on host-encoded initiation [5], all sequenced members carry conserved *gp21* homologs, implying evolutionary pressure to retain a phage-encoded helicase. We suggest that Gp21 facilitates DNA unwinding at various stages of phage replication, particularly during the transition from theta to ori-independent genome replication mode. Based on the presented findings, we propose reclassifying Gp21 as an SF4-type replicative DNA helicase. While

this study significantly enhances our understanding of *Ceduovirus* phage replication, some limitations remain. Our study lacked direct comparison to canonical SF4 DNA helicases and we employed only standard synthetic DNA substrates. Further mechanistic insights into the Gp21 functional specificity could be gained using complex or structured DNA substrates such as G-quadruplexes. *In silico* CLANS analysis positioned Gp21 on the periphery of the RepA helicase cluster, highlighting its divergence from classical SF4 proteins, including the DnaB-like helicases. Although structural modelling provides high-confidence predictions, a high-resolution structure would offer more definitive insights into Gp21 function and evolutionary origin. To our knowledge, this is the first study characterizing a replication-related protein from lactococcal *Ceduovirus* phages. The assignment of helicase activity to Gp21 provides a foundation for understanding replication in this phage group and offers broader insight into the roles of early gene products, laying the groundwork for future studies on phage biology and replication dynamics.

CRediT authorship contribution statement

Anna Santo: Writing – review & editing, Writing – original draft, Methodology, Investigation. **Magdalena Chmielewska-Jeznach:** Writing – review & editing, Methodology, Investigation. **Kamil Steczkiewicz:** Visualization, Investigation. **Tamara Aleksandrzak-Piekarczyk:** Writing – review & editing, Formal analysis, Conceptualization. **Agnieszka K. Szczepankowska:** Writing – review & editing, Writing – original draft, Supervision, Methodology, Funding acquisition, Conceptualization.

Funding

This research was supported by the National Science Center Miniatura 3 grant number 2019/03/X/NZ1/00467.

Declaration of competing interest

The authors declare that they have no known competing financial interests or personal relationships that could have appeared to influence the work reported in this paper.

Acknowledgements

We would like to thank Dr. Krzysztof Skowronek from the Biophysics and Bioanalytics Facility of the International Institute of Molecular and Cell Biology in Warsaw for assistance with SEC-MALS analysis. The CD spectropolarimeter and the ÄKTA Purifier system were sponsored in part by the Centre for Preclinical Research and Technology (CePT), a project co-sponsored by the European Regional Development Fund Innovate Economy, The National Cohesion Strategy of Poland.

Appendix A. Supplementary data

Supplementary data to this article can be found online at https://doi.org/10.1016/j.ijbiomac.2025.145668.

Data availability

The original data presented in this study are included in the article and Supplementary Material file. Any further inquiries can be directed to the corresponding author.

References

[1] S. Labrie, S. Moineau, Multiplex PCR for detection and identification of lactococcal bacteriophages, Appl. Environ. Microbiol. 66 (3) (2000) 987–994, https://doi.org/10.1128/AEM.66.3.987-994.2000.

[2] H. Brüssow, F. Desiere, Comparative phage genomics and the evolution of *Siphoviridae*: insights from dairy phages, Mol. Microbiol. 39 (2) (2001) 213–222, https://doi.org/10.1046/j.1365-2958.2001.02228.x.

[3] H. Deveau, S.J. Labrie, M.-C. Chopin, S. Moineau, Biodiversity and classification of lactococcal phages, Appl. Environ. Microbiol. 72 (6) (2006) 4338–4346, https://doi.org/10.1128/AEM.02517-05.

[4] M. Chmielewska-Jeznach, J.K. Bardowski, A.K. Szczepankowska, Molecular, physiological and phylogenetic traits of *Lactococcus* 936-type phages from distinct dairy environments, Sci. Rep. 8 (1) (2018) 12540, https://doi.org/10.1038/s41598-018-30371-3.

[5] M. Chmielewska-Jeznach, J.K. Bardowski, A.K. Szczepankowska, *Lactococcus Ceduovirus* phages isolated from industrial dairy plants-from physiological to genomic analyses, Viruses 12 (3) (2020) 280, https://doi.org/10.3390/v12030280.

[6] N.R. Waterfield, M.W. Lubbers, K.M. Polzin, R.W. Le Page, A.W. Jarvis, An origin of DNA replication from *Lactococcus lactis* bacteriophage c2, Appl. Environ. Microbiol. 62 (4) (1996) 1452–1453, https://doi.org/10.1128/aem.62.4.1452-1453.1996.

[7] M.J. Callanan, P.W. O'Toole, M.W. Lubbers, K.M. Polzin, Examination of lactococcal bacteriophage c2 DNA replication using two-dimensional agarose gel electrophoresis, Gene 278 (1–2) (2001) 101–106, https://doi.org/10.1016/s0378-1119(01)00702-8.

[8] A.H. Schiemann, J. Rakonjac, M. Callanan, J. Gordon, K. Polzin, M.W. Lubbers, P. W. O'Toole, Essentiality of the early transcript in the replication origin of the lactococcal prolate phage c2, J. Bacteriol. 186 (23) (2004) 8010–8017, https://doi.org/10.1128/JB.186.23.8010-8017.2004.

[9] A.K. Szczepanska, E. Bidnenko, D. Płochocka, S. McGovern, S.D. Ehrlich, J. Bardowski, P. Polard, M.-C. Chopin, A distinct single-stranded DNA-binding protein encoded by the *Lactococcus lactis* bacteriophage bIL67, Virology 363 (1) (2007) 104–112, https://doi.org/10.1016/j.virol.2007.01.023.

[10] J. Rakonjac, L.J.H. Ward, A.H. Schiemann, P.P. Gardner, M.W. Lubbers, P. W. O'Toole, Sequence diversity and functional conservation of the origin of replication in lactococcal prolate phages, Appl. Environ. Microbiol. 69 (9) (2003) 5104–5114, https://doi.org/10.1128/AEM.69.9.5104-5114.2003.

[11] C. Weigel, H. Seitz, Bacteriophage replication modules, FEMS Microbiol. Rev. 30 (3) (2006) 321–381, https://doi.org/10.1111/j.1574-6976.2006.00015.x.

[12] K. Wegrzyn, I. Konieczny, Toward an understanding of the DNA replication initiation in bacteria, Front. Microbiol. 14 (2024) 1328842, https://doi.org/10.3389/fmicb.2023.1328842.

[13] H.C. Blaine, L.A. Simmons, C.L. Stallings, Diverse mechanisms of helicase loading during DNA replication initiation in bacteria, J. Bacteriol. 205 (4) (2023) e0048722, https://doi.org/10.1128/jb.00487-22.

[14] A.J. Fernandez, J.M. Berger, Mechanisms of hexameric helicases, Crit. Rev. Biochem. Mol. Biol. 56 (6) (2021) 621–639, https://doi.org/10.1080/10409238.2021.1954597.

[15] M.E. O'Donnell, H. Li, The ring-shaped hexameric helicases that function at DNA replication forks, Nat. Struct. Mol. Biol. 25 (2) (2018) 122–130, https://doi.org/10.1038/s41594-018-0024-x.

[16] M.R. Singleton, M.S. Dillingham, D.B. Wigley, Structure and mechanism of helicases and nucleic acid translocases, Annu. Rev. Biochem. 76 (2007) 23–50, https://doi.org/10.1146/annurev.biochem.76.052305.115300.

[17] G. Ziegelin, E. Scherzinger, R. Lurz, E. Lanka, Phage P4 alpha protein is multifunctional with origin recognition, helicase and primase activities, EMBO J. 12 (9) (1993) 3703–3708, https://doi.org/10.1002/j.1460-2075.1993.tb06045.x.

[18] A.K. Byrd, K.D. Raney, Superfamily 2 helicases, Front. Biosci. (Landmark Ed) 17 (6) (2012) 2070–2088, https://doi.org/10.2741/4038.

[19] K.D. Raney, A.K. Byrd, S. Aarattuthodiyil, Structure and mechanisms of SF1 DNA helicases, Adv. Exp. Med. Biol. 767 (2013) 17–46, https://doi.org/10.1007/978-1-4614-5037-5_2.

[20] S.S. Patel, K.M. Picha, Structure and function of hexameric helicases, Annu. Rev. Biochem. 69 (2000) 651–697, https://doi.org/10.1146/annurev.biochem.69.1.651.

[21] P. Fernández-Millán, M. Lázaro, Ş. Cansız-Arda, J.M. Gerhold, N. Rajala, C. A. Schmitz, C. Silva-Espiña, D. Gil, P. Bernadó, M. Valle, J.N. Spelbrink, M. Solà, The hexameric structure of the human mitochondrial replicative helicase Twinkle, Nucleic Acids Res. 43 (8) (2015) 4284–4295, https://doi.org/10.1093/nar/gkv189.

[22] H. Zhang, Z. Zhang, J. Yang, Z.G. He, Functional characterization of DnaB helicase and its modulation by single-stranded DNA binding protein in *Mycobacterium tuberculosis*, FEBS J. 281 (4) (2014) 1256–1266, https://doi.org/10.1111/febs.12703.

[23] S. Ayora, F. Weise, P. Mesa, A. Stasiak, J.C. Alonso, *Bacillus subtilis* bacteriophage SPP1 hexameric DNA helicase, G40P, interacts with forked DNA, Nucleic Acids Res. 30 (11) (2002) 2280–2289, https://doi.org/10.1093/nar/30.11.2280.

[24] A.J. Oakley, A structural view of bacterial DNA replication, Protein Sci. 28 (6) (2019) 990–1004, https://doi.org/10.1002/pro.3615.

[25] A.W. Kulczyk, C.C. Richardson, The replication system of bacteriophage T7, Enzymes 39 (2016) 89–136, https://doi.org/10.1016/bs.enz.2016.02.001.

[26] T.C. Mueser, J.M. Hinerman, J.M. Devos, R.A. Boyer, K.J. Williams, Structural analysis of bacteriophage T4 DNA replication: a review in the Virology Journal series on bacteriophage T4 and its relatives, Virol. J. 7 (2010) 359, https://doi.org/10.1186/1743-422X-7-359.

[27] Y.J. Jeong, M.K. Levin, S.S. Patel, The DNA-unwinding mechanism of the ring helicase of bacteriophage T7, Proc. Natl. Acad. Sci. USA 101 (19) (2004) 7264–7269, https://doi.org/10.1073/pnas.0400372101.

[28] H. Zhang, S.J. Lee, A.W. Kulczyk, B. Zhu, C.C. Richardson, Heterohexamer of 56- and 63-kDa gene 4 helicase-primase of bacteriophage T7 in DNA replication,

J. Biol. Chem. 287 (41) (2012) 34273–34287, https://doi.org/10.1074/jbc.M112.401158.
[29] T. Lionnet, M.M. Spiering, S.J. Benkovic, D. Bensimon, V. Croquette, Real-time observation of bacteriophage T4 gp41 helicase reveals an unwinding mechanism, Proc. Natl. Acad. Sci. USA 104 (50) (2007) 19790–19795, https://doi.org/10.1073/pnas.0709793104.
[30] F. Dong, P.H. von Hippel, The ATP-activated hexameric helicase of bacteriophage T4 (gp41) forms a stable primosome with a single subunit of T4-coded primase (gp61), J. Biol. Chem. 271 (32) (1996) 19625–19631, https://doi.org/10.1074/jbc.271.32.
[31] K. El Omari, C. Meier, D. Kainov, G. Sutton, J. Grimes, M. Poranen, D. Bamford, R. Tuma, D. Stuart, E. Mancini, Tracking in atomic detail the functional specializations in viral RecA helicases that occur during evolution, Nucleic Acids Res. 41 (20) (2013) 9396–9410, https://doi.org/10.1093/nar/gkt713.
[32] M. Hall, S. Matson, Helicase motifs: the engine that powers DNA unwinding, Mol. Microbiol. 34 (5) (2000) 867–877, https://doi.org/10.1046/j.1365-2958.1999.01659.x.
[33] M.T. Washington, A.H. Rosenberg, K. Griffin, F.W. Studier, S.S. Patel, Biochemical analysis of mutant T7 primase/helicase proteins defective in DNA binding, nucleotide hydrolysis, and the coupling of hydrolysis with DNA unwinding, J. Biol. Chem. 271 (43) (1996) 26825–26834, https://doi.org/10.1074/jbc.271.43.26825.
[34] M.R. Sawaya, S. Guo, S. Tabor, C.C. Richardson, T. Ellenberger, Crystal structure of the helicase domain from the replicative helicase-primase of bacteriophage T7, Cell 99 (2) (1999) 167–177, https://doi.org/10.1016/s0092-8674(00)81648-7.
[35] I. Donmez, S.S. Patel, Mechanisms of a ring shaped helicase, Nucleic Acids Res. 34 (15) (2006) 4216–4224, https://doi.org/10.1093/nar/gkl508.
[36] G. Ziegelin, T. Niedenzu, R. Lurz, W. Saenger, E. Lanka, Hexameric RSF1010 helicase RepA: the structural and functional importance of single amino acid residues, Nucleic Acids Res. 31 (20) (2003) 5917–5929, https://doi.org/10.1093/nar/gkg7905.
[37] C. Schouler, S.D. Ehrlich, M.-C. Chopin, Sequence and organization of the lactococcal prolate-headed bIL67 phage genome, Microbiology (Reading) 140 (Pt11) (1994) 3061–3069, https://doi.org/10.1099/13500872-140-11-3061.
[38] UniProt Consortium, UniProt: the universal protein knowledgebase in 2023, Nucleic Acids Res. 51 (D1) (2023) D523–D531, https://doi.org/10.1093/nar/gkac1052.
[39] J. Wang, F. Chitsaz, M.K. Derbyshire, N.R. Gonzales, M. Gwadz, S. Lu, G. H. Marchler, J.S. Song, N. Thanki, R.A. Yamashita, M. Yang, D. Zhang, C. Zheng, C. J. Lanczycki, A. Marchler-Bauer, The conserved domain database in 2023, Nucleic Acids Res. 51 (D1) (2023) D384–D388, https://doi.org/10.1093/nar/gkac1096.
[40] S.R. Eddy, Accelerated profile HMM searches, PLoS Comput. Biol. 7 (10) (2011) e1002195, https://doi.org/10.1371/journal.pcbi.1002195.
[41] L. Zimmermann, A. Stephens, S.Z. Nam, D. Rau, J. Kübler, M. Lozajic, F. Gabler, J. Söding, A.N. Lupas, V. Alva, A completely reimplemented MPI bioinformatics toolkit with a new HHpred server at its core, J. Mol. Biol. 430 (15) (2018) 2237–2243, https://doi.org/10.1016/j.jmb.2017.12.007.
[42] J. Abramson, J. Adler, J. Dunger, et al., Accurate structure prediction of biomolecular interactions with AlphaFold 3, Nature 630 (8016) (2024) 493–500, https://doi.org/10.1038/s41586-024-07487-w.
[43] K. Katoh, K. Misawa, K. Kuma, T. Miyata, MAFFT: a novel method for rapid multiple sequence alignment based on fast Fourier transform, Nucleic Acids Res. 30 (14) (2002) 3059–3066, https://doi.org/10.1093/nar/gkf436.
[44] T. Frickey, A. Lupas, CLANS: a Java application for visualizing protein families based on pairwise similarity, Bioinformatics 20 (18) (2004) 3702–3704, https://doi.org/10.1093/bioinformatics/bth444.
[45] M.J. Gasson, Plasmid complements of *Streptococcus lactis* NCDO 712 and other lactic streptococci after protoplast-induced curing, J. Bacteriol. 154 (1) (1983) 1–9, https://doi.org/10.1128/jb.154.1.1-9.1983.
[46] M.R. Green, J. Sambrook, Transformation of *Escherichia coli* by electroporation, Cold Spring Harb Protoc 6 (2020) 101220, https://doi.org/10.1101/pdb.prot101220.
[47] C.L. Kielkopf, W. Bauer, I.L. Urbatsch, Bradford assay for determining protein concentration, Cold Spring Harb Protoc 4 (2020) 102269, https://doi.org/10.1101/pdb.prot102269.
[48] E. Curti, S.J. Smerdon, E.O. Davis, Characterization of the helicase activity and substrate specificity of *Mycobacterium tuberculosis* UvrD, J. Bacteriol. 189 (5) (2007) 1542–1555, https://doi.org/10.1128/JB.01421-06.
[49] A. Savitzky, M.J.E. Golay, Smoothing and differentiation of data by simplified least squares procedures, Anal. Chem. 36 (8) (1964) 1627–1639, https://doi.org/10.1021/ac60214a047.
[50] J.A. Morrow, M.L. Segall, S. Lund-Katz, M.C. Phillips, M. Knapp, B. Rupp, K. H. Weisgraber, Differences in stability among the human apolipoprotein E isoforms determined by the amino-terminal domain, Biochemistry 39 (38) (2000) 11657–11666, https://doi.org/10.1021/bi000099m.
[51] A.M. Krishnan, L.M. Burroughs, L. Aravind Iyer, Comprehensive classification of ABC ATPases and their functional radiation in nucleoprotein dynamics and biological conflict systems, Nucleic Acids Res. 48 (18) (2020) 10045–10075, https://doi.org/10.1093/nar/gkaa726.
[52] E.V. Koonin, Y.I. Wolf, L. Aravind, Protein fold recognition using sequence profiles and its application in structural genomics, Adv. Protein Chem. 54 (2000) 245–275, https://doi.org/10.1016/s0065-3233(00)54008-x.
[53] E. Scherzinger, G. Ziegelin, M. Bárcena, J.M. Carazo, R. Lurz, E. Lanka, The RepA protein of plasmid RSF1010 is a replicative DNA helicase, J. Biol. Chem. 272 (48) (1997) 30228–30236, https://doi.org/10.1074/jbc.272.48.30228.
[54] V. Rajagopal, S.S. Patel, Viral Helicases. Viral Genome Replication 1 (2008) 429–466, https://doi.org/10.1007/b135974_20.
[55] M.K. Levin, M. Gurjar, S.S. Patel, A Brownian motor mechanism of translocation and strand separation by hepatitis C virus helicase, Nat. Struct. Mol. Biol. 12 (5) (2005) 429–435, https://doi.org/10.1038/nsmb920.
[56] J.A. Sommers, L.N. Loftus, M.P. Jones 3rd, R.A. Lee, C.E. Haren, A.J. Dumm, R. M. Brosh Jr., Biochemical analysis of SARS-CoV-2 Nsp13 helicase implicated in COVID-19 and factors that regulate its catalytic functions, J. Biol. Chem. 299 (3) (2023) 102980, https://doi.org/10.1016/j.jbc.2023.102980.
[57] M.K. Levin, M.M. Gurjar, S.S. Patel, ATP binding modulates the nucleic acid affinity of hepatitis C virus helicase, J. Biol. Chem. 278 (26) (2003) 23311–23316, https://doi.org/10.1074/jbc.M301283200.
[58] A.K. Satapathy, D.J. Crampton, B.B. Beauchamp, C.C. Richardson, Promiscuous usage of nucleotides by the DNA helicase of bacteriophage T7: determinants of nucleotide specificity, J. Biol. Chem. 284 (21) (2009) 14286–14295, https://doi.org/10.1074/jbc.M900557200.
[59] F.G. Harmon, S.C. Kowalczykowski, Biochemical characterization of the DNA helicase activity of the *Escherichia coli* RecQ helicase, J. Biol. Chem. 276 (1) (2001) 232–243, https://doi.org/10.1074/jbc.M006555200.
[60] D.J. Crampton, M. Ohi, U. Qimron, T. Walz, C.C. Richardson, Oligomeric states of bacteriophage T7 gene 4 primase/helicase, J. Mol. Biol. 360 (3) (2006) 667–677, https://doi.org/10.1016/j.jmb.2006.05.037.
[61] W. Bujalowski, M.M. Klonowska, M.J. Jezewska, Oligomeric structure of *Escherichia coli* primary replicative helicase DnaB protein, J. Biol. Chem. 269 (50) (1994) 31350–31358.
[62] F. Dong, E.P. Gogol, P.H. von Hippel, PH., The phage T4-coded DNA replication helicase (Gp41) forms a hexamer upon activation by nucleoside triphosphate, J. Biol. Chem. 270 (13) (1995) 7462–7473, https://doi.org/10.1074/jbc.270.13.7462.
[63] J. Chase, A. Catalano, A.J. Noble, E.T. Eng, P.D. Olinares, K. Molloy, D. Pakotiprapha, M. Samuels, B. Chait, A. des Georges, D. Jeruzalmi, Mechanisms of opening and closing of the bacterial replicative helicase, Elife 7 (2018) e41140, https://doi.org/10.7554/eLife.41140.
[64] P. Ahnert, K.M. Picha, S.S. Patel, A ring-opening mechanism for DNA binding in the central channel of the T7 helicase-primase protein, EMBO J. 19 (13) (2000) 3418–3427, https://doi.org/10.1093/emboj/19.13.3418.
[65] K. Ciechanowska, A. Szczepanska, K. Szpotkowski, K. Wojcik, A. Urbanowicz, A, Kurzynska-Kokorniak, The human Dicer helicase domain is capable of ATP hydrolysis and single-stranded nucleic acid binding. BMC Biol. 22 (1) (2024) 287, https://doi.org/10.1186/s12915-024-02082-x.